Chemical Engineering Journal Advances 25 (2026) 100991

Contents lists available at ScienceDirect

Chemical Engineering Journal Advances

journal homepage: www.sciencedirect.com/journal/chemical-engineering-journal-advances

Improving fouling resistance of polyvinylidene fluoride membrane with mono-hydroxyl poly(dimethylsiloxane) (PDMS-OH) grafted silica nanoparticles

Muayad Al-Shaeli [a,e], Raed A. Al-Juboori [b], Huanting Wang [c], Bradley Ladewig [a,*], Qusay F. Alsalhy [d,*], Jianhua Zhang [e]

[a] Paul Wurth Chair, Faculty of Science, Technology and Medicine, University of Luxembourg, 2, Avenue de l'Université, L-4365 Esch-sur-Alzette, Luxembourg
[b] Water and Environmental Engineering Research Group, Department of Built Environment, Aalto University, Espoo, Finland
[c] Monash university, department of chemical engineering, Australia
[d] Membrane Technology Research Unit, Chemical Engineering Department, University of Technology-Iraq, Alsena'a Street 52, Baghdad 10066, Iraq
[e] Institute for Sustainability and Innovation, Victoria University, P.O. Box 14428, Melbourne, Victoria 8001, Australia

ARTICLE INFO

Keywords:
PVDF membrane
Silica nanoparticles
Monohydroxy polydimethylsiloxane
Steglich esterification
Fouling resistance
Protein rejection

ABSTRACT

In this study, mono-hydroxyl polydimethylsiloxane (CH_3-PDMS-OH) was successfully grafted onto silica (SiO_2) nanoparticles via Steglich esterification process to produce surface-functionalized PDMS-g-SiO_2 nanomaterials. These nanoparticles were then introduced into polyvinylidene fluoride (PVDF) matrices through non-induced phase inversion (NIPS) to fabricate mixed matrix ultrafiltration membranes with different nanoparticle loadings (0, 1.6, 3.2, 6.3, and 11.8 wt %). The PDMS-g-SiO_2 incorporation resulted in membranes with slightly reduced porosity and hydrophobicity compared to pristine PVDF yet exhibited markedly improved antifouling performance. Although pure water flux decreased slightly due to the addition of nanoparticles, the rejection rate of Bovine serum albumin (BSA) improved substantially because of optimized pore structure and surface chemistry. In contrast, membranes containing unmodified SiO_2 showed higher initial flux but suffered from severe irreversible fouling. The modified PVDF membranes showed a flux recovery ratio of up to 97 % and significantly reduced protein adsorption (19.9 μg/cm^2) relative to pristine PVDF (62 μg/cm^2), confirming the formation of a low-energy, fouling-resistant surface. High flux recovery was sustained over four fouling/cleaning cycles with both BSA and humic acid (HA), and its durability was further demonstrated through 15 days of long-term testing. This study establishes a new hybrid design approach that combines the hydrophobic flexibility of PDMS with the hydrophilic stability of SiO_2, offering a durable and effective route for developing antifouling PVDF membranes for wastewater treatment applications.

1. Introduction

Membrane filtration is one of the most promising technologies for treating water sources with various qualities due to its high separation efficiency and low energy consumption [1–3]. Ultrafiltration (UF) membranes, in particular, efficiently remove dissolved matter, colloidal, and microbial contaminants under low transmembrane pressures (<5 bar), making them widely used in wastewater treatment and related industrial processes [4,5–8]. However, their practical application is restricted by membrane fouling, which is a major problem that reduces performance and increases maintenance costs [9–11]. Fouling occurs primarily through the adsorption and accumulation of proteins and biomacromolecules on the membrane surface and within its pores, leading to severe flux decline, shortened membrane lifespan, and increased operational expenses [12–14].

Polyvinylidene fluoride (PVDF) is one of the most widely utilized polymers for UF membrane fabrication because of its excellent chemical resistance, mechanical strength, thermal stability, and tolerance toward oxidizing and corrosive media [15–19]. Despite these outstanding properties, PVDF membranes are more prone to organic and biofouling. This is mainly attributed to their hydrophobic CH_2–CF_2 backbone, which presents a low-surface-energy interface that facilitates foulant adhesion [20,21]. Thus, enhancing the antifouling performance of PVDF membranes requires strategies that modify the membrane surface to improve

* Corresponding authors.
E-mail addresses: bradley.ladewig@uni.lu (B. Ladewig), qusay_alsalhy@yahoo.com (Q.F. Alsalhy).

https://doi.org/10.1016/j.ceja.2025.100991

Available online 10 December 2025

hydrophilicity, reduce fouling interactions, or otherwise alter surface characteristics to resist contaminant accumulation [20–22]. Several strategies have been explored to address PVDF fouling. One common approach is physical blending or surface grafting with hydrophilic polymers such as polyethylene glycol (PEG)-based materials [23], zwitterion-based materials [24], and hydrophilic nanoparticles (e.g., SiO_2) [25]. Additionally, engineering the surface topography of membranes has been shown to influence fouling behavior. For example, membranes with roughened surfaces or low-modulus coatings can enhance shear-induced foulant detachment, reducing fouling adhesion and accumulations [26–28].

Fluorinated polymers have traditionally served as antifouling coatings due to their low surface energy; however, environmental concerns related to the leaching of perfluorinated compounds have encouraged the search for safer and environmentally friendly alternatives. Polydimethylsiloxane (PDMS) has emerged as a promising candidate for membrane modification due to its low toxicity, excellent chemical stability, and high flexibility [29,30]. The antifouling behavior of PDMS is largely attributed to the rotational flexibility of its Si–O backbone, which reduces the binding strength between surface contaminants and the membrane, facilitating foulant removal under shear flow. However, direct blending of PDMS into polymer matrices often suffers from several limitations, including poor interfacial compatibility, uneven surface distribution, and potential leaching during membrane operation [31–34]. To overcome these limitations, hybrid systems combining inorganic nanoparticles with PDMS, or other hydrophobic or hydrophilic polymers have been explored, which improve nanoparticle dispersion, interfacial stability, and overall membrane performance [35,36].

In this work, we propose a novel solution entails the synthesis and the incorporation of mono-hydroxyl polydimethylsiloxane (PDMS-OH) grafted silica nanoparticles (PDMS-g-SiO_2 NPs) into PVDF membranes to enhance its antifouling properties. Unlike conventional modification approaches such as PEGylation [23], zwitterionic coatings [24], or incorporation of hydrophilic nanoparticles [25], this work introduces a dual character nanohybrid system that combines hydrophobic PDMS chains and hydrophilic SiO_2 moieties at the nanoscale. This hybrid system enables a balance of surface energy and controlled surface segregation within the PVDF matrix, resulting in improved fouling resistance without excessive hydrophilization that could otherwise compromise mechanical strength or cause pore collapse. An additional advantage of this approach is the use of PDMS-OH rather than the more commonly employed di-hydroxyl PDMS (e.g., Wang et al., 2016 [37]). The former allows for a single-point grafting onto SiO_2 nanoparticles via Steglich esterification, producing pendant PDMS chains that remain surface-active during membrane formation. This design promotes the preferential migration of PDMS toward the membrane-water interface, forming a hydrophobic, low-surface-energy layer that reduces fouling, while maintaining stable nanoparticle dispersion within the PVDF matrix

This approach addresses two major scientific gaps in PDMS-based antifouling membranes: 1) It prevents PDMS leaching and phase separation, which are common in physically blended PDMS-PVDF systems, by covalently anchoring PDMS onto SiO_2 nanoparticles 2) It achieves synergistic antifouling behavior through the coexistence of hydrophilic (Si–OH) and hydrophobic (Si-CH_3) functionalities, balancing water affinity with foulant repellence at the membrane surface. The incorporation of PDMS-g-SiO_2 into PVDF membrane was examined through a set of analytical tests and the performance of the synthesized membranes and their antifouling properties were evaluated using common model foulants such as Humic acid (HA) and (Bovine serum albumin) BSA.

2. Experimental work

2.1. Materials used

Commercial SiO_2 (fumed) nanoparticles was obtained from Sigma Aldrich, Australia. It was mono dispersed 7 nm (0.007 μm) and had a surface area of 395 ± 25 m^2/g. Polyvinylidene fluoride (PVDF Solef 6020, Mn = 313 kDa) was purchased from Solvay and dried at 55 °C for 12 h before use. Lithium Chloride (LiCl, purity ≥ 99.99 %, from Sigma Aldrich) was used as pore-forming agent and dried in oven at 90 °C for 12 h before use. N, N-dimethylacetamide (DMAc, purity ≥ 99 %, from Sigma Aldrich), 3-(triethoxysilyl) propionitrile (TESPN, purity 97 %, from Sigma Aldrich), N, N'-diisopropylcarodiimide (DIC, purity 99 %, from Sigma Aldrich), 4-dimethylaminopyridine (DMAP, purity 98 %, from Fluka), polyethylene glycol (PEG, from Sigma Aldrich), sodium hydroxide pellets (NaOH, from Merck Millipore), and polydimethylsiloxane monohydroxy terminated (PDMS-OH, Mw = 4000 Da, from Sigma Aldrich) were used as received. Bovine serum albumin (BSA, 68 kDa, agarose gel electrophoresis, from Sigma Aldrich) was used as a model foulant during ultrafiltration experiments.

2.2. Synthesis of PDMS-g-SiO_2 nanoparticles

PDMS-g-SiO_2 nanoparticles were prepared by a three-step synthesis method, including silane coupling, functional group hydrolysis, and finally Steglich esterification, as described by Wu and co-workers [38]. First, 2 g of fumed silica nanoparticles were functionalised with TESPN (a nitrile terminated silane coupling agent) at 57 °C. Exposed nitrile groups were then hydrolysed to carboxylic acid by presence of HCl/Milli-Q water (50:50) vol % at 72.5 °C for 12 h under gentle stirring, providing a reaction site for subsequent esterification. In the third step, 338.4 mg (i.e., 0.0828 mmol) mono-hydroxyl (terminal) functionalised PDMS (PDMS-OH) was attached to 0.3 g carboxylic acid functionalised silica nanoparticles by a Steglich esterification with 10.45 mg (i.e., 0.0828 mmol) N, N'-diisopropylcarbodiimide (DIC) (coupling agent), in the presence of 5.06 mg (i.e., 0.0414 mmol) 4-dimethylaminopyridine (DMAP) as illustrated in Fig. 1.

2.3. Preparation of mixed matrix PVDF membranes

In this study, mixed matrix PVDF UF membranes were prepared using a non-solvent induced phase separation (NIPS) method. For each membrane, casting solutions were prepared by dissolving different amounts of PDMS-g-SiO_2 (0, 1.6, 3.2, 6.3, 11.8 %) in 16 mL DMAc, which was then sonicated for 20 min. To this solution, 0.426 g of LiCl was then added, followed by 3.2 g of PVDF and the mixture was stirred overnight at 200 rpm. Casting solution compositions are detailed in Table 1. After mixing, the casting solution was left covered overnight in the fumehood until no air bubbles were presented. The solution was then cast using a glass plate and a casting knife (supplied by Paul Gardner CO., Inc.) with a 150 μm gap. Then, the membranes were immersed in a deionized water bath until the membrane solidified. After solidification, the membranes were washed successively with double deionized water (DDI) and kept in fresh DDI before use [30,39]. The resultant series of membranes were labelled PVDF+LiCl (control), SiO_2PDMS$_x$PVDF, where x is the mass fraction of PDMS-g-SiO_2 filler in the PVDF based membranes.

2.4. Characterization

The structural properties of the prepared membranes were characterized employing a range of analytical tools. Fourier Transform Infrared spectroscopy (FTIR-ATR) at a resolution of 4 cm^{-1} and an average of 64 scans and a range of 4000–600 cm^{-1} was utilized to track the changes in the functional groups of the membranes. Surface and cross-sectional micrographs were obtained by Scanning Electron Microscopy

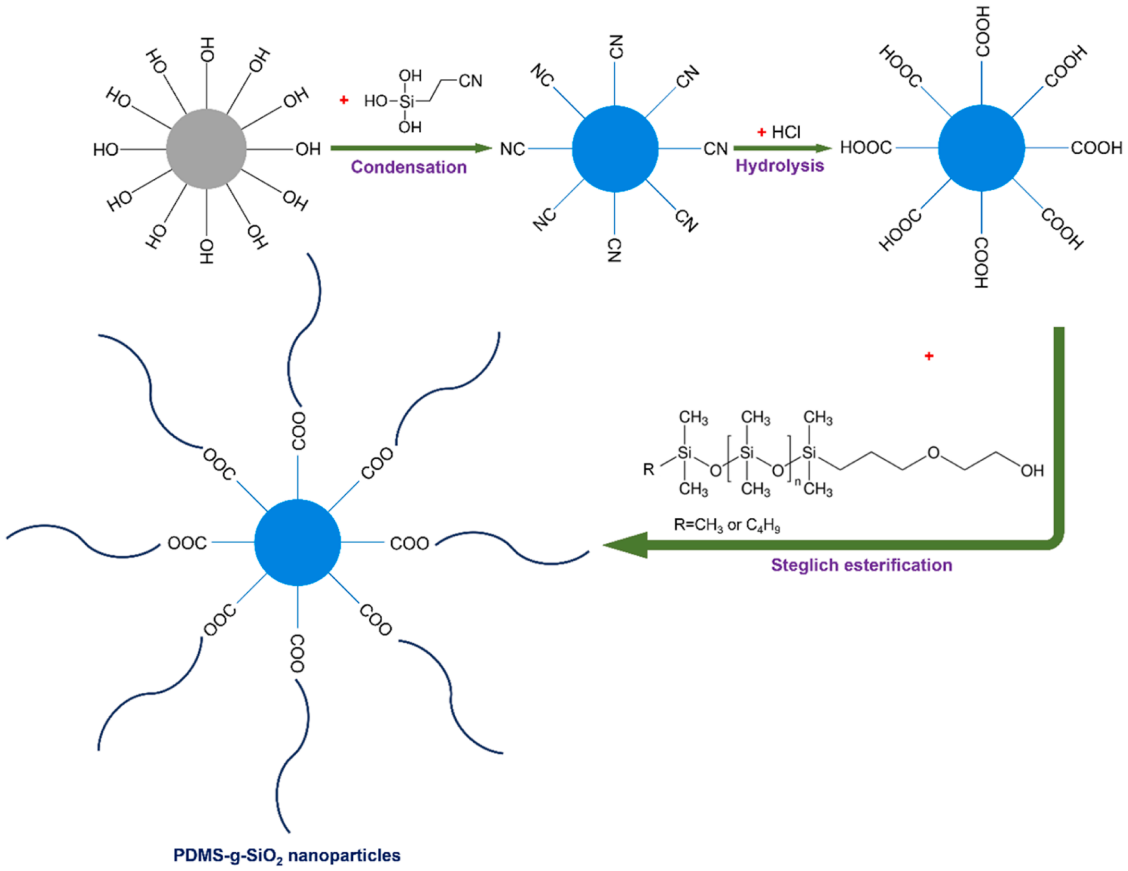

Fig. 1. Schematic diagram illustration of grafting mono-hydroxyl (PDMS-OH) chain on the surface of SiO_2 NPs.

Table 1
Recipes for preparing the hybrid membranes.

Membrane	PVDF	LiCl	DMAC	PDMS-g-SiO_2 (In casting solution)	PDMS-g-SiO_2 (in membrane)
PVDF +LiCl	15	2.0	83.00	0	0
$SiO_2PDMS_{0.25\ \%}$ PVDF	15	2.0	82.75	0.25	1.6
$SiO_2PDMS_{0.5\ \%}$ PVDF	15	2.0	82.50	0.5	3.2
$SiO_2PDMS_{1.0\ \%}$ PVDF	15	2.0	82.00	1.0	6.3
$SiO_2PDMS_{2\ \%}$ PVDF	15	2.0	81.00	2.0	11.8

Note: the numbers given in Table 1 correspond to percentage by mass. Composition of nanocomposite membrane calculated from polymer: additive ratio of the casting solution, assuming complete incorporation of PMDS-g-SiO_2.

(Magellan SEM, FEI company, America). SEM samples were prepared by drying them first at room temperature and then sputter coating with a 0.5 nm layer of Iridium (208HR sputter coater, Cressington, UK). For cross-section morphology, small pieces of prepared membranes were immersed in liquid nitrogen for 1.5 min and then the samples were frozen and fractured. The samples were then fixed on SEM holder using double-sided carbon tape and coated with Ir. Elemental analysis of the prepared membrane was characterized using EDX equipped Nova NanoSEM 450 (Quantax 400 X-ray analysis system, Bruker, USA). The surface structure of the pristine and modified PVDF membranes was characterized by X-ray photoelectron spectroscopy (XPS) using an AXIS Nova spectrometer (Kratos Analytical Inc., Manchester, UK) with a monochromated Al Kα source at a power of 180 W (15 kV × 12 mA) and a hemispherical analyzer operating in the fixed analyzer transmission mode.

Thermal stability of the prepared membranes was measured using a TA instrument 2950 thermogravimetric analyzer (TGA). Small pieces of membranes were loaded into a high temperature platinum pan. Nitrogen gas was used gas at flow rate of 2–2.5 cm^3/min. The membrane samples were heated at a rate of 20 °C/min up-1000 °C under oxygen atmosphere at flow rate of 10 cm^3/min. Thermogravimetric analysis (TGA) was further employed to calculate the surface grafting density of PDMS on the PVDF membranes. The surface grafting density (σ) was estimated using the following expression, adapted from previous literature: [40, 41]

$$\sigma = \frac{m_{PDMS} \times N_A}{M_{monomer} \times A} \quad (1)$$

Where: $m_{PDMS:}$ is the mass of PDMS determined from TGA (mg)

$M_{monomer}$ is the molecular weight of the PDMS repeating unit (–Si–O–CH_3, 74 g/mol)

A is the effective membrane surface area (m^2)

N_A: is Avogadro's number

To measure the membrane hydrophilicity, water contact angles (CA) of the membranes surface were measured using the sessile drop technique (PGX+, Fibro System Ab, Sweden). Membrane samples were cut from the prepared samples and fix on slide glass using double side tape. A 5 μL of distilled water was dropped onto the membrane sample through the microsyringe in air. At least 5 measurements of contact angle were recorded for each membrane sample to enhance the reliability and an average data was reported. Membrane porosity was calculated using a gravimetric method. A piece of the prepared membrane was immersed in water for 3 h and W_w was taken. The wet piece was then drying in vacuum oven at 60 °C and W_D was weighed. The porosity was calculated according to Eq. (2) [42,43].

$$\varepsilon\ (\%) = \frac{\frac{W_w - W_D}{D_w}}{\frac{W_w - W_D}{D_w} + \frac{W_D}{D_p}} \quad (2)$$

where W_D is the weight of the dry membrane (g), W_w is the weight of the wet membrane (g) and D_w & D_p and are the densities of the water and polymer (g cc^{-1}).

Solute rejection and molecular weight cut-off (MWCO) were determined using a series of 1 g/L of polyethylene glycol (PEG) solutions, prepared by adding PEG of varying molecular weight (35, 100, 200 kDa) to deionized water. PEG rejection rates were calculated from the concentrations of PEG in the feed solution (C_f) and permeate water (C_P) using a total organic carbon analyzer (TOC-LCSH, Shimadzu, Japan). The pore size of the membranes was then estimated based on the values of MWCO of the membrane according to the Eq. (3) [44].

$$r = 0.262\sqrt{\mathrm{MWCO}} - 0.3 \quad (3)$$

where r = pore size of membrane (nm), MWCO= molecular weight cut-off (g mol^{-1}). MWCO was calculated by interpolating measured rejection rate to a rejection of 90 %.

Pure water flux (PWF) of the virgin and modified PVDF membranes were measured using dead-end cell filtration unit (HP4750 stirred cell, Sterlitech, USA). The membrane samples were cut to a diameter of 49 mm and an effective membrane area of 14.6 cm^2. The filtration cell was filled with DDI and then connected to small tank with 5 L water. The system has been compressed by nitrogen gas cylinder to push the water passing through the membrane. The collected permeate was measured using a digital balance with mass change automatically recorded with connected Labview software. At the beginning of the experiments, membrane samples were first precompacted at 150 kPa for at least 1 h to stabilize the flux, which is then recorded at a pressure of 100 kPa (J_{w1}). At least five membrane samples were tested, and an average was taken to get accurate data. Constant transmembrane Pressure mode was used in this study to determine the fouling resistance of the membranes.

A BSA solution was placed in the filtration cell (1 g/L, prepared in advance using phosphate buffer saline, pH = 7.4) and pressurized at 100 kPa for 1 h. The BSA flux (J_{BSA}) was recorded at the last 10 min of the 1 h running.

The concentrations of BSA concentrations in the feed and permeates side was spectroscopically measured at 280 nm using Varian Cary 100 Bio UV–VIS spectrophotometer. The protein rejection ratio (%R) of the membrane was calculated by the equation below (4) [45]:

$$\%\ R = \left(1 - C_P/C_f\right) \times 100 \quad (4)$$

where *R(%)* is the rejection coefficient of the membrane, C_f and C_P (mg/mL) were the protein concentration of feed and permeate stream and the concentration of BSA in the solution was calculated based on the calibration curve prepared in advance.

After testing, the fouled membranes were cleaned. For physical cleaning, DDI was used to wash the membranes. The membranes were added to the filtration cell and washed three times with DDI for 20 min. The water flux was recorded after physical cleaning of membranes. For chemical cleaning, 100 mL of NaOH solution (2 g L^{-1}, pH=12) was added to the filtration cell and stirred for 20 min before being washed three times with DDI to remove the NaOH solution. After each cleaning step, the membrane flux was recorded at 100 kPa (J_{w2}). flux recovery ratio of membranes was calculated to evaluate the membrane operation as shown in the following Eq. (5):

$$FRR\ (\%) = \frac{J_{W2}}{J_{W1}} \times 100 \quad (5)$$

To study the membrane fouling in detail, total fouling resistance (R_t), reversible fouling resistance (R_r) and irreversible fouling resistance (R_{ir}) were determined using the following equations respectively [46].

$$R_t = \frac{J_{W1} - J_{BSA}}{J_{W1}} \times 100 \quad (6)$$

$$R_r = \frac{J_{W2} - J_{BSA}}{J_{W1}} \times 100 \quad (7)$$

$$R_{ir} = \frac{J_{W1} - J_{W2}}{J_{W1}} \times 100 \quad (8)$$

where J_p: is the flux of BSA foulant model. R_t is the sum of R_r and R_{ir}.

Static protein adsorption experiments were conducted to determine the amount of protein adsorbed on the surface of membrane. The top surface of membranes ($\varnothing$ = 25 mm diameter) was exposed to BSA solution (1 g/L) in a filtration cell. The cell was then incubated in a shaker (operated at 150 rpm) at room temperature and 24 h to reach the adsorption–desorption equilibrium. The amount of protein adsorbed was calculated using the following equation.

$$Q = \frac{(C_a - C_b)V}{A} \quad (9)$$

where Q = protein adsorbed (μg.cm^{-2}), C_a= original conc of BSA (g L^{-1}) C_b = final concentration of BSA (g L^{-1}), A = area of membranes (cm^2), V = volume of BSA solution (L).

The concentration of BSA was determined based on the absorbance at 280 nm using a UV spectroscope (UV mini-1240 spectrophotometer, Shimadzu, Japan). At least three membranes were tested for each sample and an average data was taken. After experiment of static protein, the flux for the fouled membrane was recorded. The BSA fouled membranes were cleaned physically and chemically and the flux was recorded again at 100 kPa. The flux recovery ratio was calculated again using equation 4

3. Results and discussion

3.1. Characterization of silica NPs before and after modifications

The FTIR spectra of pristine SiO_2 and PDMS-grafted SiO_2 nanoparticles (PDMS-g-SiO_2) are presented in Fig. 2a. Both samples exhibit prominent absorption bands at approximately 1060 cm^{-1} and 800 cm^{-1}, corresponding to the Si–O–Si and Si–O stretching vibrations, respectively, which are characteristic of the silica network [45–48]. These peaks confirm the presence of the silica network structure in both samples. After modification with PDMS, a new and distinct absorption band appears at 2960 cm^{-1}, which corresponds to the asymmetric stretching vibration of methyl groups (–CH_3) present in the PDMS chains [48,49]. Although this peak is relatively weak due to the low concentration of grafted organic content compared to the dominant inorganic silica framework, its presence is significant because it does not appear in the pristine SiO_2 spectrum. This subtle but consistent shift confirms the successful chemical attachment of PDMS to the silica surface. Additionally, a weak carbonyl peak at 1652 cm^{-1} is observed, which may be attributed to unreacted PDMS-OH or ester linkage by-product formed during the Steglich esterification process.

While the overall spectral contrast before and after grafting may appear modest due to overlapping silica signals and low PDMS loading, the emergence of –CH_3 and C=O signals, even as minor features strongly support the occurrence of surface grafting. These findings align with previous studies where similar low-intensity signals were observed indicating successful surface modification of nanoparticles [50].

The results of gravimetric analysis of bare SiO_2 and PDMS-g-SiO_2 NPs are shown in Fig. 2b The pure silica exhibited typical minimal weight loss curve with two loss stages [51]: 30–100 °C which is attributed to the loss of physically and chemically adsorbed water (via hydrogen bonding) [52], and 100–400 °C which could be a result of organic contaminants. In comparison, PDMS-g-SiO_2 NPs exhibited a higher

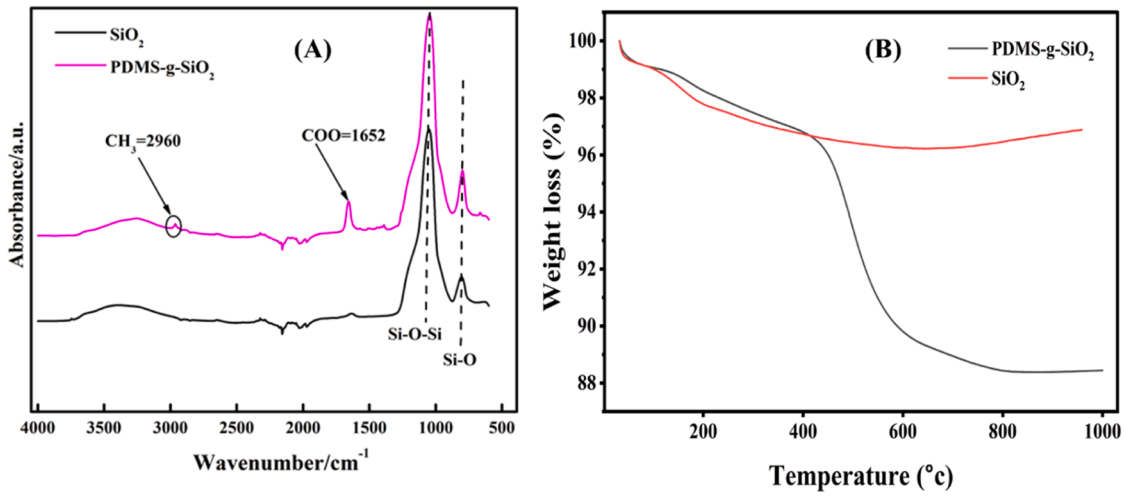

Fig. 2. Structural properties of SiO_2 nanoparticles: (A) FTIR-ATR spectra, (B) TGA curves.

weight loss with three stages of which the first and second stages were the same as SiO_2. The third stage represents the thermal decomposition of PDMS-g-SiO_2 NPs which occurred between ≈ 350–800 ºC with the weight loss of ≈ 10 %. Based on previous reports, the thermal degradation of PDMS polymer at around 336 ºC [38]. At the temperature range of 700–1000 °C, a very weight gain was observed, and this phenomenon could be due to the partially reaction of decomposed bridging organic groups with oxygen [53]. This result is in line with the previous reports [40]. After grafting SiO_2 with PDMS, The TGA analysis result proved the successful grafting of PDMS on the surface of SiO_2 NPs.

These physicochemical characterizations collectively confirm that PDMS chains were successfully anchored onto the SiO_2 nanoparticles, providing a hybrid material with both hydrophobic (PDMS) and hydrophilic (SiO_2) characteristics. Such dual functionality is expected to play a critical role in the subsequent membrane fabrication, where the modified nanoparticles may preferentially migrate toward the membrane surface during phase inversion method. After establishing the physical parameters that affect the membrane formation process, it is important to understand how the incorporation of PDMS-g-SiO_2 nanoparticles modifies the chemical structure and morphology of the PVDF

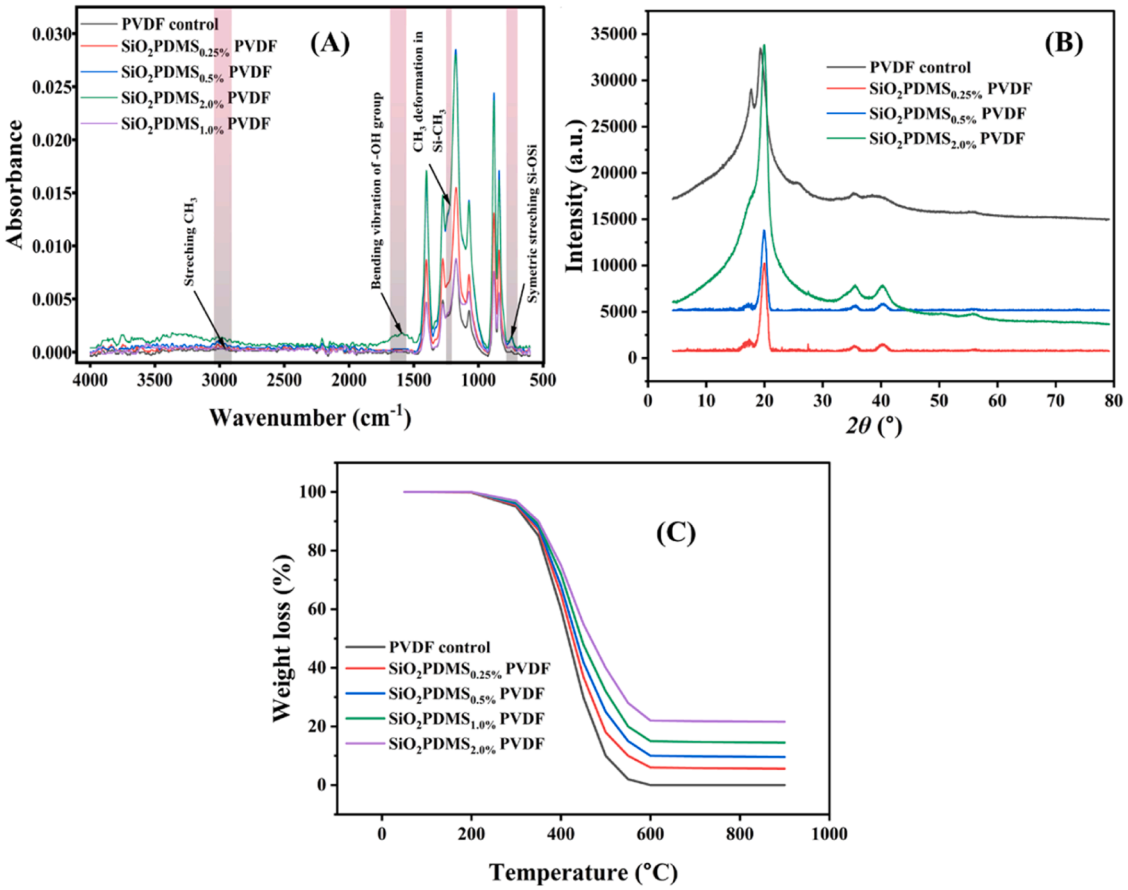

Fig. 3. Control PVDF and mixed matrix PVDF membranes characteristics (A) FTIR-ATR (B) XRD spectra and (C) TGA analysis.

membranes. Therefore, in the following section, detailed characterization analyses for the PVDF membranes are presented to correlate structural changes with the observed macroscopic membrane properties.

3.2. Characterization of hybrid membranes

To examine the impact of incorporating PDMS-g-SiO_2 nanoparticles on the chemical structure of PVDF mixed matrix membranes, FTIR-ATR spectrum was conducted, and the resulting spectra are shown in Fig. 3A. All membranes, including the pristine PVDF and those modified with different PDMS-g-SiO_2 loadings (0.25–2 wt. %), display characteristic PVDF peaks at 1174 cm^{-1} and 1275 cm^{-1}, corresponding to the symmetric and asymmetric stretching vibrations of C–F bonds, and at 1405 cm^{-1}, attributed to the bending vibration of the $–CH_2$ groups. These characteristic peaks confirm that the fundamental PVDF backbone structure is preserved upon the incorporation of PDMS-g-SiO_2 nanoparticles [54]. With increasing PDMS-g-SiO_2 content, a gradual improvement in peak intensity is observed in the 800 cm^{-1} region, which can be associated with the overlapping Si–O–Si stretching vibrations of the silica framework and the Si–O–C linkages from the PDMS segments [55,56]. The other observed changes include the shoulder growth around 1260 cm-1 which is relate to the methyl deformation in Si-CH_3 characteristic of PDMS structure [56]. The peak around 1620 cm^{-1} which is likely attributed to the bending vibration of OH group absorbed on SiO_2 surface [51] became more prominent especially with the highest PDMS-g-SiO_2 load. The subtle peak growth accompanying the increase in NPs load around 2900 cm^{-1} could be attributed to CH_3 stretching in Si-CH_3 of PDMs [56]. The FTIR analysis confirms the successful integration of PDMS-g-SiO_2 into PVDF and the preservation of the backbone of the latter.

The XRD patterns presented in Fig. 3B illustrate the changes in crystallinity of control PVDF membrane as opposed to the modified membranes with various concentrations of SiO_2-PDMS nanoparticles (0.25 %, 0.5 %, and 2 %). The control PVDF membrane exhibits distinct and broad diffraction peaks centered around 2θ values of approximately 18.5°, 20.1°, and 26.6°, which are typical for the α-phase crystalline structure of PVDF. These sharp peaks indicate a semi-crystalline structure, with the 20.1° peak particularly corresponding to the (110)/(200) planes. With the addition of SiO_2-PDMS nanoparticles, a progressive reduction in peak intensity and sharpness is observed. This reduction becomes more significant as the nanoparticle concentration increases, especially in the case of the SiO_2PDMS$_{2\ \%}$ PVDF membrane. The broadening and weakening of the diffraction peaks suggest a decrease in the overall crystallinity of the polymer matrix. The reduction in crystallinity is attributed to the disruptive influence of the PDMS-grafted silica nanoparticles on the regular packing and crystallization of the PVDF chains. Additionally, two small broad peaks appeared upon the addition of SiO_2PDMS around 35° and 40° which were also reported by another study that examined SiO_2 incorporation into PVDF [57] and may correspond to the amorphous or weakly crystalline domains of the SiO_2 nanoparticles.

XPS was used to study the surface composition and confirm the incorporation of PDMS-g-SiO_2 nanoparticles within the PVDF membrane matrix. Tables 2 and 3 present the surface elemental composition and the binding energies of the different structural moieties of both control and modified membranes. The control PVDF membrane displayed only C (52.8 %) and F (47.2 %) signals, characteristic of the PVDF backbone with no detectable Si or O peaks. In contrast, the PDMS-g-SiO_2 modified membranes showed new Si2p peaks (~103 eV) and O1s peaks (~532 eV), attributed to Si-O-Si and O-Si-C bonds, confirming the successful incorporation of PDMS-g-SiO_2 at the membrane surface. The surface atomic concentrations of Si and O increased progressively with higher nanoparticle loading, from 2.7 % and 8.7 % at 0.5 wt. % to 7.4 % and 15.2 % at 2 wt. %, respectively. Correspondingly, the F content decreased from 39.1 % to 33.1 %, while the C content slightly decreased,

Table 2
XPS surface elemental composition of PVDF and PDMS-g-SiO_2 membranes.

Sample	% Si	%O	%C	%F	Interpretation
PVDF control	0	0	52.8	47.2	PVDF+LiCl, no Si/O signals
SiO_2PDMS$_{0.5\ \%}$ PVDF	2.7	8.7	49.5	39.1	Appearance of Si and O peaks confirms PDMS–SiO_2 at the surface
SiO_2PDMS$_{1.0\ \%}$ PVDF	4.5	11.5	47.2	36.8	Increasing Si and O content with decreasing F surface enrichment
SiO_2PDMS$_{2.0\ \%}$ PVDF	7.4	15.2	44.3	33.1	Strong Si2p and O1s peaks; significant fluorine reduction indicates PDMS–SiO_2 dominance at the outer surface.

Table 3
XPS core-level binding energies of pristine and PDMS-g-SiO_2-Modified PVDF membranes.

Sample	Element	% Atomic	Binding Energies (eV)	Assignment / Observation
Control PVDF	C 1s	52.4	284.8	C–C, C–H from PVDF backbone
	F 1s	44.7	688.5	C–F from PVDF backbone
	O 1s	2.9	532.3	Surface oxidation / adventitious O (not intrinsic)
SiO_2 NPs	Si 2p	31.6	103.3	Si–O–Si
	O 1s	68.4	532.8	Si–O
SiO_2PDMS$_{0.5\ \%}$ PVDF	C 1s	49.8	284.8(C–C/C–H), 283.2 (C–Si)	PDMS backbone formation (Si–C)
	F 1s	42.5	688.4	C–F (PVDF)
	Si 2p	4.1	101.8	Si–C (PDMS), Si–O–Si
	O 1s	3.6	532.7	Si–O, Si–OH
SiO_2PDMS$_{1.0\ \%}$ PVDF	Si 2p	4.5	101.9 (Si–C), 103.2 (Si–O–Si)	Increasing Si and O content with decreasing F surface enrichment
	O 1s	11.5	532.6	Si–O–Si, Si–OH from PDMS-g-SiO_2
	C 1s	47.2	284.8 (C–C/C–H), 283.2 (C–Si)	PDMS backbone (surface segregation)
	F 1s	36.8	688.5	C–F from PVDF
SiO_2PDMS$_{2.0\ \%}$ PVDF	C 1s	47.9	284.8 (C–C/C–H), 283.2 (C–Si)	Strong PDMS signal (surface enrichment)
	F 1s	40.6	688.5	C–F from PVDF
	Si 2p	6.2	101.8(Si–C), 103.3 (Si–O–Si)	Strong PDMS-g-SiO_2 signal
	O 1s	5.3	532.6	Si–O–Si

reflecting the partial replacement of PVDF backbone at the surface by PDMS–SiO_2 nanoparticles. This compositional shift toward higher Si and O levels at the membrane surface indicates strong surface enrichment of PDMS-g-SiO_2, consistent with the preferential migration of the low-surface-energy PDMS segments during the phase inversion process.

To evaluate the thermal stability of the fabricated PVDF and PVDF-PDMS-g-SiO_2 membranes, thermogravimetric analysis was conducted (Fig. 3C) under a nitrogen atmosphere from 25 to 900 °C at a heating rate of 15 °C/min. The TGA results showed that pure PVDF undergoes significant thermal degradation starting around 350 °C, with rapid weight loss observed between 400 °C and 500 °C [58,59]. By 600 °C, the pure PVDF had almost completely decomposed, leaving negligible residue, which is consistent with its typical two-step degradation behavior involving dehydrofluorination and main chain scission. In contrast, the PVDF membranes modified with PDMS-g-SiO_2 nanoparticles demonstrated improved thermal stability, with degradation occurring more gradually and at slightly higher temperatures compared to the virgin

PVDF. As the concentration of PDMS-g-SiO_2 increased from 0.25 wt % to 2.0 wt %, the thermal degradation shifted to higher temperatures and the residual weight at 900 °C increased significantly. For example, the residual mass for the PVDF with 2.0 wt % PDMS-g-SiO_2 was approximately 21.6 %, compared to 5.6 % for the membrane with only 0.25 wt % loading. This enhancement can be attributed to the thermally stable silica nanoparticles, which act as inorganic fillers that resist decomposition and slow the diffusion of volatile degradation products. Additionally, the inherent thermal resistance of PDMS, due to its siloxane backbone, further delays the polymer degradation. The observed increase in residual weight with higher nanoparticle loading confirms that a larger fraction of thermally stable inorganic content remains after the polymer matrix decomposes. Overall, these results demonstrate that incorporating PDMS-g-SiO_2 into the PVDF matrix significantly improves thermal resistance, making the membranes more suitable for applications involving elevated temperatures.

TGA further corroborated the presence of PDMS at the membrane surface and provided a basis to estimate the grafting density [60]. In the TGA curves of the PDMS-g-SiO_2 membranes, the decomposition of PDMS was identified as the weight loss occurring between 200 °C and 500 °C, a temperature range where PVDF remains largely stable. The mass loss in this range was attributed specifically to the PDMS component, giving ~0.29 mg for the 0.5 % PDMS-g-SiO_2 membrane (sample mass = 5.10 mg: effective membrane area = 14.6 cm^2). Similarly, the 1 % and 2 % PDMS-g-SiO_2 membranes exhibited PDMS weight losses of 0.49 mg and 0.74 mg, respectively. Using the molecular weight of the PDMS repeating unit (–Si–O–CH_3, 74 g/mol), these values correspond to surface grafting densities of approximately 0.54, 0.84, and 1.01 mmol/m^2, or equivalently ~1.6 × 10^3, 2.7 × 10^3, and 4.1 × 10^3 molecules/nm^2. This analysis confirms progressive surface attachment and increasing grafting density with higher nanoparticle loading, consistent with the preferential migration of PDMS-g-SiO_2 toward the membrane–water interface.

Building upon the structural and compositional findings obtained from FTIR, XRD, and XPS analyses, the surface and cross-sectional morphologies of the fabricated membranes were further examined using SEM and EDX to elucidate how the introduction of PDMS-g-SiO_2 nanoparticles influences the overall membrane architecture Fig. 4 (A–F). The SEM micrographs clearly reveal morphological changes on the membrane surface as the concentration of PDMS-g-SiO_2 nanoparticles increases. Particularly at higher loadings of 1 % and 2 %, the silica nanoparticles become more apparent, suggesting that these particles tend to migrate toward the membrane surface during the phase inversion process. This migration is likely driven by thermodynamic forces and interfacial energy differences, which favor the accumulation of nanoparticles at interfaces such as the membrane–air or membrane–solvent boundaries. Consequently, this redistribution of nanoparticles affects the membrane's internal microstructure, leading to a denser and more mechanically robust architecture, while also influencing surface properties relevant to antifouling.

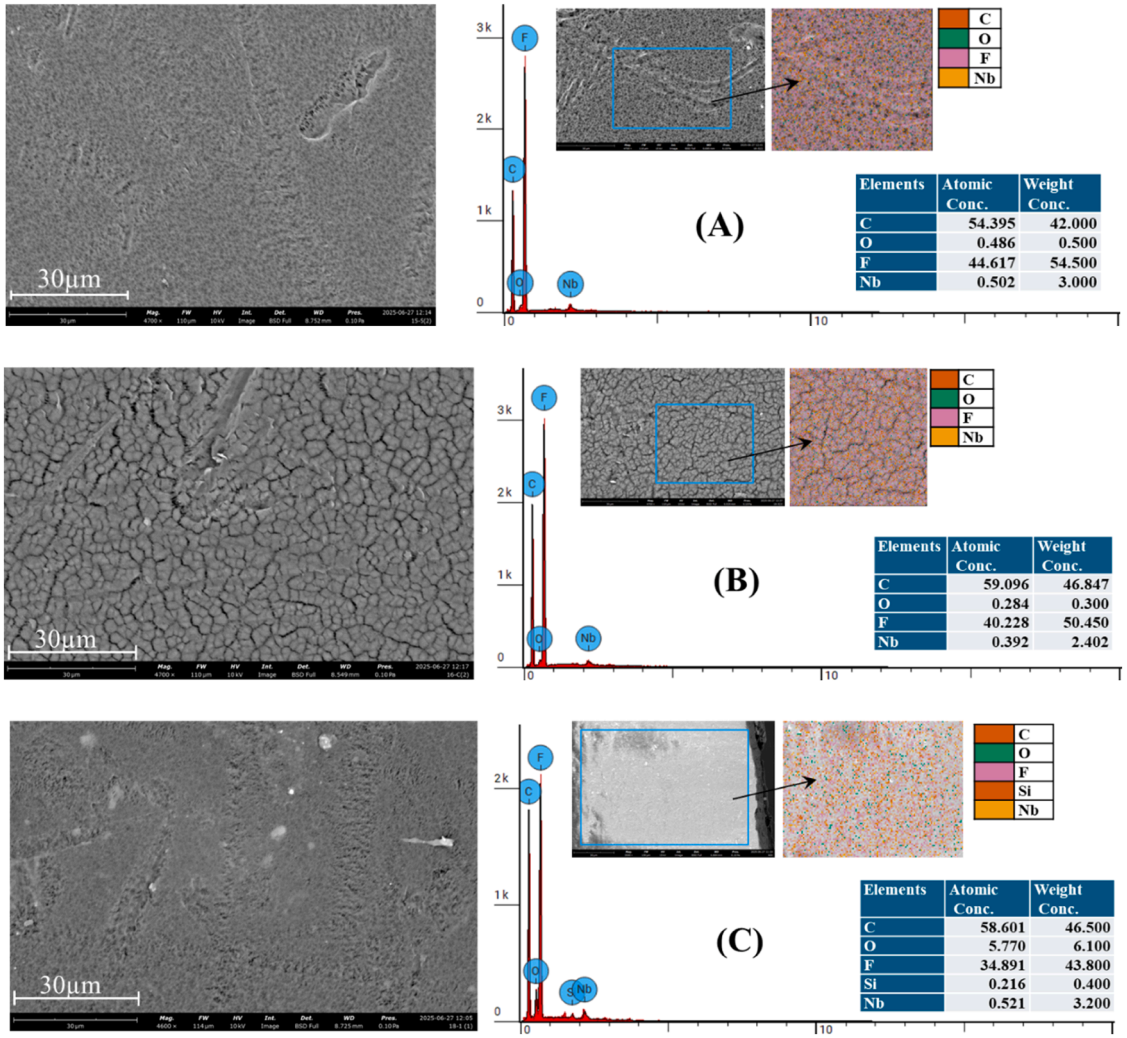

Fig. 4. SEM top surface morphology and EDS elemental mapping of (A) pristine PVDF, (B) PVDF control, (C) $SiO_2PDMS_{0.25\ \%}$ PVDF, (D) $SiO_2PDMS_{0.5\ \%}$ PVDF, (E) $SiO_2PDMS_{1.0\ \%}$ PVDF, and (F) $SiO_2PDMS_{2.0\ \%}$ PVDF.

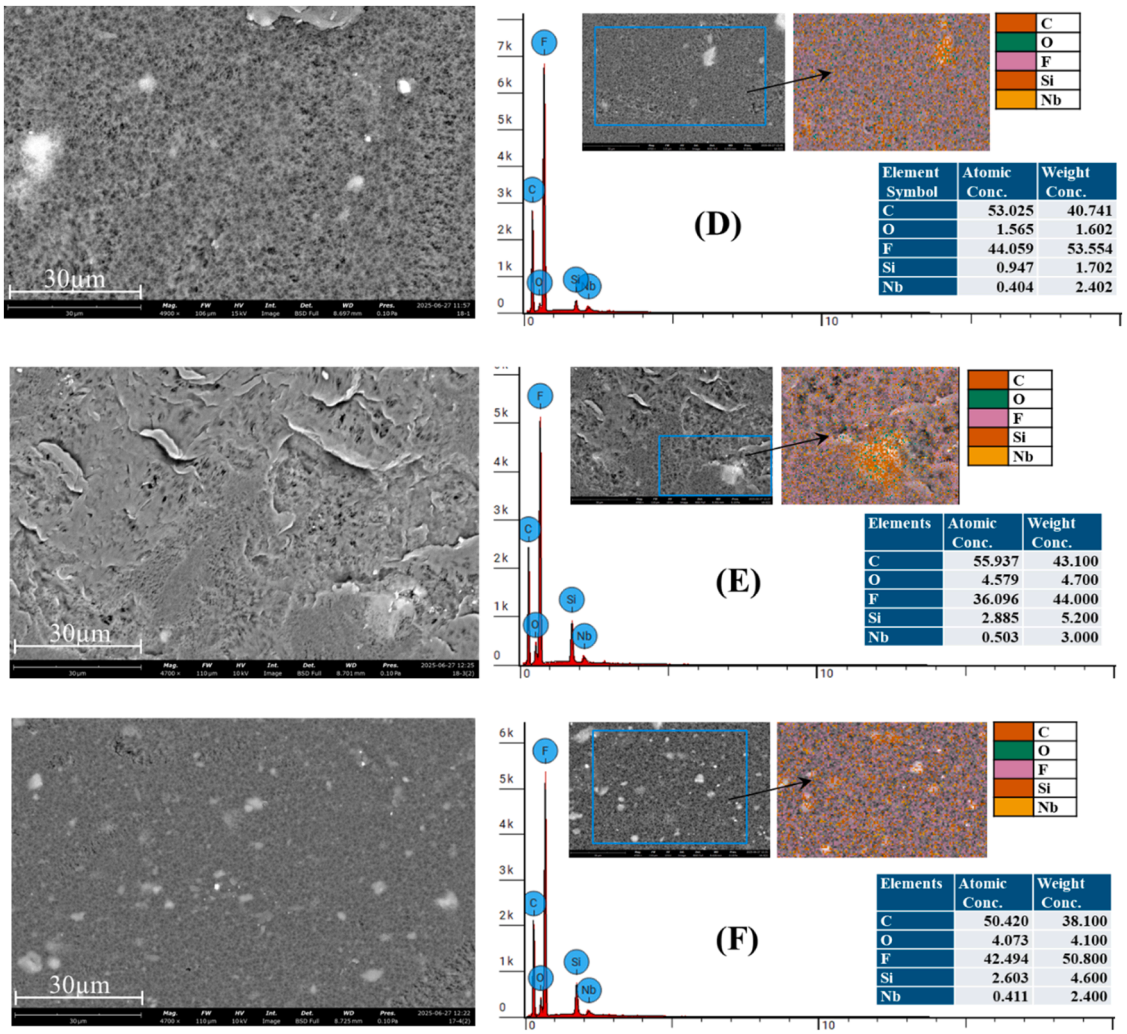

Fig. 4. (*continued*).

The corresponding EDX spectra further validate the successful incorporation of PDMS-g-SiO_2 into the PVDF matrix. Distinct peaks are observed for carbon (C) at approximately 0.3 keV and fluorine (F) at around 0.7 keV, which are characteristic signals from the PVDF polymer. More importantly, the presence of a silicon (Si) peak at roughly 1.75 keV provides strong evidence for the successful integration of SiO_2 nanoparticles onto the membrane surface. A detectable oxygen (O) signal is also present, which may originate from both the silica framework and oxygen-containing side groups in the PVDF or PDMS structures. The EDX elemental mapping shows that silica is distributed across the surface in aggregates of NPs. The Si signal increases proportionally with increasing the loading percentage with slight deviation in high percentages.

Fig. 5 compares the cross-sectional SEM morphologies of pristine and modified PVDF membranes, revealing that PDMS-g-SiO_2 loading strongly influences the internal structure. The pristine PVDF membrane (Fig. 5A) displays a typical asymmetric structure formed by the NIPS process, consisting of a dense skin layer followed by short finger-like macrovoids and a porous sublayer. Upon nanoparticle incorporation (Fig. 5B–E), the skin layer becomes denser, and the finger-like macrovoids extend deeper into the sublayer, gradually transforming into a sponge-like morphology. These structural changes are attributed to increased solution viscosity and altered demixing kinetics caused by the PDMS-g-SiO_2 nanoparticles, which slow solvent–nonsolvent exchange and promote more controlled phase separation. This microstructural evolution corroborates the XRD observation of reduced crystallinity and the XPS evidence of surface enrichment, suggesting that the presence of PDMS-g-SiO_2 not only modifies polymer chain packing but also governs the membrane's hierarchical morphology. These morphological refinements directly influence key surface-related properties, such as wettability, porosity, and pore size distribution, which consequently affect the separation performance of the membranes and their fouling propensity.

The surface wettability of UF membranes plays a crucial role in determining their separation efficiency and resistance to fouling. This property is commonly evaluated using water CA measurements, where a lower contact angle indicates higher surface hydrophilicity and improved wettability. As shown in Table 4, the pristine PVDF membrane exhibited a contact angle of 89.3°, indicating moderate hydrophilicity. Upon incorporation of LiCl, CA dropped to 75.4 (Tables 3 and S1). However, the addition of PDMS-g-SiO_2 increased it gradually as the loading percentage increased but always lower than that of pristine PVDF. This increase in contact angle suggests a slight decline in hydrophilicity, which can be attributed to the inherently hydrophobic nature of PDMS chains grafted onto the silica nanoparticles. PDMS is known for its low surface energy and non-polar methyl groups, which tend to migrate toward the membrane surface during phase inversion [61]. This migration changes the membrane's surface chemistry, increasing CA. Furthermore, the difference in surface free energy between the PVDF polymer and the PDMS-modified nanoparticles leads to interfacial rearrangements, which further influence the surface wettability.

While the observed change in contact angle reflects the surface

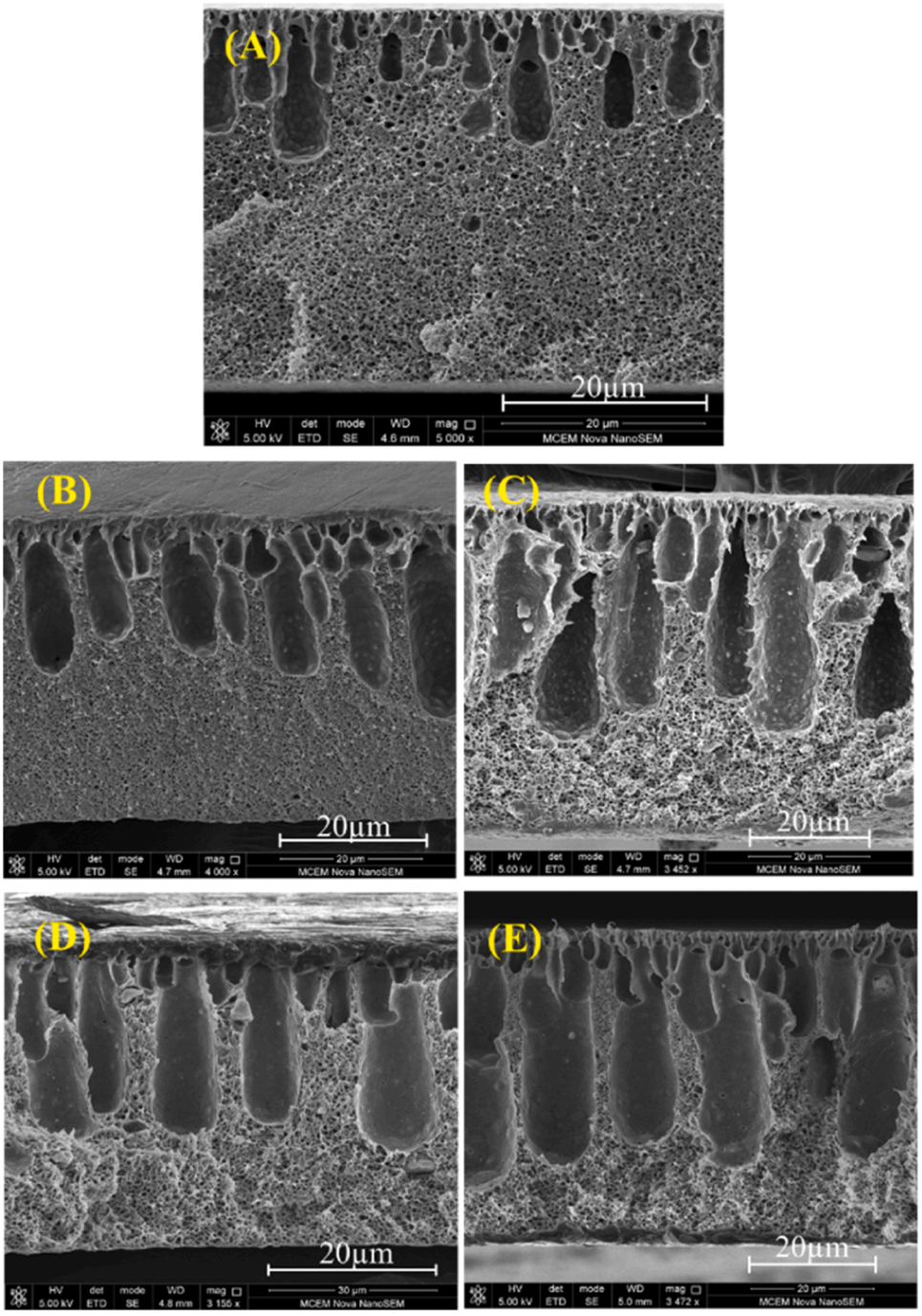

Fig. 5. SEM cross-section images of (A) control PVDF membrane. (B) SiO_2PDMS$_{0.25\ \%}$PVDF membrane (C) SiO_2PDMS$_{0.5\ \%}$PVDF membrane (D) SiO_2PDMS$_{1.0\ \%}$PVDF membrane (E) SiO_2PDMS$_{2.0\ \%}$PVDF membrane.

Table 4
Viscosity, Porosity, contact angle, MWCO, pore size and thickness for unmodified and PVDF membranes with modified SiO_2.

Membranes	Viscosity (mPa.s)	Porosity (%)	Contact angle (deg)	MWCO (KDa)	Pore size (nm)	Thickness of membrane (µm)
PVDF +LiCl (control)	620	85.3 ± 0.8	75.4 ± 1.2	188	22.1 ± 0.4	45.00±1.20
SiO_2PDMS$_{0.25\ \%}$ PVDF	680	83.8 ± 1.0	77.7 ± 0.3	186	21.8 ± 0.5	49.11±1.35
SiO_2PDMS$_{0.5\ \%}$ PVDF	745	80.3 ± 0.9	78.0 ± 0.7	182	21.7 ± 0.4	55.39±1.45
SiO_2PDMS$_{1.0\ \%}$ PVDF	845	79.9 ± 1.1	80.5 ± 0.8	180	21.6 ± 0.3	54.32±1.28
SiO_2PDMS$_{2\ \%}$ PVDF	970	78.0 ± 1.2	82.9 ± 1.3	178	21.1 ± 0.5	56.35±1.50

chemistry alteration, the structural characteristics, particularly pore size and porosity also provide essential insight into how nanoparticle incorporation affects overall membrane morphology and transport behavior. The mean surface pore size of membranes (Table 4) reduced slightly from 22.1 nm for control PVDF to 21.1 nm for SiO_2PDMS_2 %PVDF membrane when the contents of PDMS-g-SiO_2 increased. The porosity of membranes also decreased from about 85 % for control PVDF to 78 % for SiO_2PDMS_2 %PVDF. The results reveal a progressive decrease in both pore size and porosity with increasing nanoparticle content. The overall porosity of the membranes decreased from 85.3 % for pristine PVDF to ≈78.0 % for the membrane with 2 % PDMS-g-SiO_2, consistent with the trend observed for unmodified and modified silica particles (Tables 4 and S1). This reduction in pore size and porosity correlates well with the morphological observations from SEM images and can be mechanistically explained by changes in the phase inversion dynamics caused by the nanoparticles. The decrease of porosity and pore size could lead to lower flux of the modified membranes (as illustrated in Fig. 6).

As nanoparticle loading increases particularly with PDMS chains grafted on SiO_2, the viscosity of the casting solution rises, which slows down the solvent (DMAc) non-solvent (water) exchange during phase inversion method. This delayed demixing reduces the formation of large pores and favors the development of denser membrane structures with smaller average pore diameters. Consequently, slower phase separation kinetics and inhibited macrovoid formation yield tighter membrane structures with fewer interconnected voids. This change in the mixing dynamics also led to membrane thickness increase from 45.00 μm for the pristine PVDF to 56.35 μm at 2 % loading. The skin layer thickness though not directly measured rather inferred from the SEM images (Fig. 5) became denser and more compact with increased nanoparticle loading.

In summary, the integration of PDMS-g-SiO_2 nanoparticles modifies both the surface and internal morphology of PVDF membranes. The balance between hydrophobic PDMS segments and hydrophilic silica cores leads to subtle structural rearrangements that simultaneously influence wettability, pore formation, and mechanical integrity laying the foundation for the enhanced antifouling and separation performance discussed in the following sections.

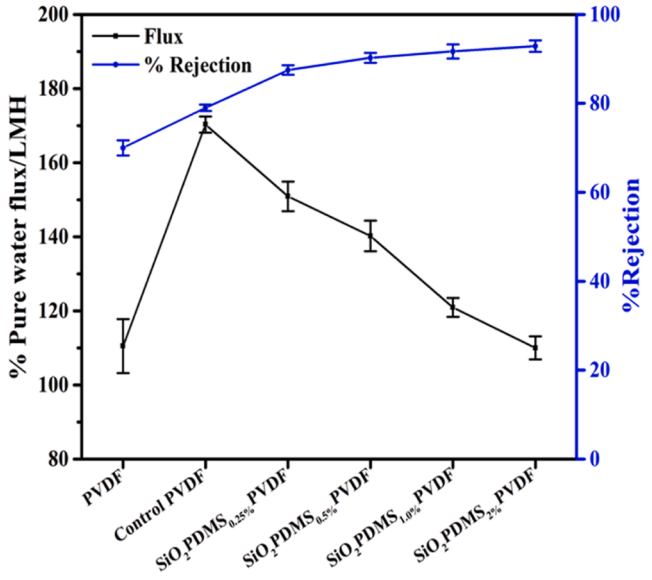

Fig. 6. Pure water flux and % BSA rejection of virgin PVDF and mixed matrix PVDF UF membranes. 1 g L^{-1} BSA was chosen as the feed solution and all filtration tests were conducted at a transmembrane pressure of 100 kPa. Error bars represent the standard deviation of triplicate measurements.

3.3. Separation performance of hybrid membranes

The performance data illustrated in Fig. 6 highlights the influence of PDMS-grafted SiO_2 nanoparticles on the separation efficiency of PVDF membranes. The pure water flux initially increases for the control PVDF membrane when compared to the unmodified PVDF, which can be attributed to the presence of LiCl acting as a pore-forming agent during membrane fabrication. This results in a more porous structure and reduced resistance to water flow, thereby improving flux. However, as PDMS-g-SiO_2 nanoparticles were introduced and their concentration increased from 0.25 % to 2 %, a gradual decline in pure water flux was observed. This trend is primarily due to an increase in the viscosity of the casting solution (Table 2), which alters the dynamics of the solvent–non-solvent exchange (NIPS) process. The elevated viscosity slows down the NIPS process, leading to the formation of a denser skin layer and resulting in membranes with lower porosity and smaller pore sizes [50]. These structural changes increase the resistance to water permeation, thereby reducing flux.

The BSA rejection efficiency increases consistently with the rise in PDMS-g-SiO_2 content (as shown in Fig. 6). This improvement can be attributed to the reduction in pore size, which strengthens size exclusion of protein aggregates. The surface modification also contributes to improved antifouling properties through alterations in surface energy and interfacial interactions, leading to greater selectivity. The hydrophilic nature of the silica core combined with the low-surface-energy PDMS chains produces a more fouling-resistant surface, thereby increasing BSA rejection. Electrostatic repulsion further contributes to the enhanced BSA rejection of the modified membranes. Since the isoelectric point of BSA lies in the range of 4.7–5.2 [62], the protein carries a net negative charge under the neutral pH conditions applied in this study. Meanwhile, silanol (Si–OH) groups on the nanoparticle surface deprotonate to form silanolate ($Si–O^-$) species [63] which increases the negative charge of the membrane and consequently promoting BSA rejection through electrostatic repulsion [64]. Such repulsive interactions positively influence the antifouling behavior observed in the flux recovery tests presented in the following section.

Another contributing factor to the improved BSA rejection is the increased membrane thickness in the modified samples (Table 4), which provides additional resistance to protein permeation [65]. The increased rejection percentage, exceeding 95 % at the highest nanoparticle concentration, underscores the significance of both structural and surface modifications in improving membrane selectivity. In contrast, the composite PVDF membranes containing unmodified SiO_2 nanoparticles display a decline in BSA rejection (Table S1), further emphasizing the beneficial role of PDMS grafting.

Overall, the results show a clear trade-off between permeability and fouling resistance, a well-recognized phenomenon in polymeric composite membranes. The inclusion of PDMS-grafted nanoparticles introduces a dual effect: (i) an increase in casting solution viscosity (Table 2) and the development of a denser surface morphology (Fig. 5) that restricts water permeation, and (ii) the migration of PDMS segments to the surface (Fig. 4), forming a flexible and low-surface-energy layer that reduces protein adsorption and fouling adhesion. Although this structural rearrangement leads to a moderate reduction in water flux, it provides significant long-term operational advantages by minimizing irreversible fouling (Table 4) and sustaining effective flux recovery. Hence, the PDMS-g-SiO_2 nanocomposite PVDF membranes demonstrate an optimized balance between transport and fouling resistance a relationship consistent with previous studies on PDMS- and PEG-modified PVDF systems [22,26]. Thus, the transition from unmodified PVDF to PDMS-g-SiO_2 hybrid membranes clearly reveals how surface functionalization systematically tunes both structural and separation performance, ultimately linking flux behavior, rejection efficiency, and antifouling durability in a coherent framework.

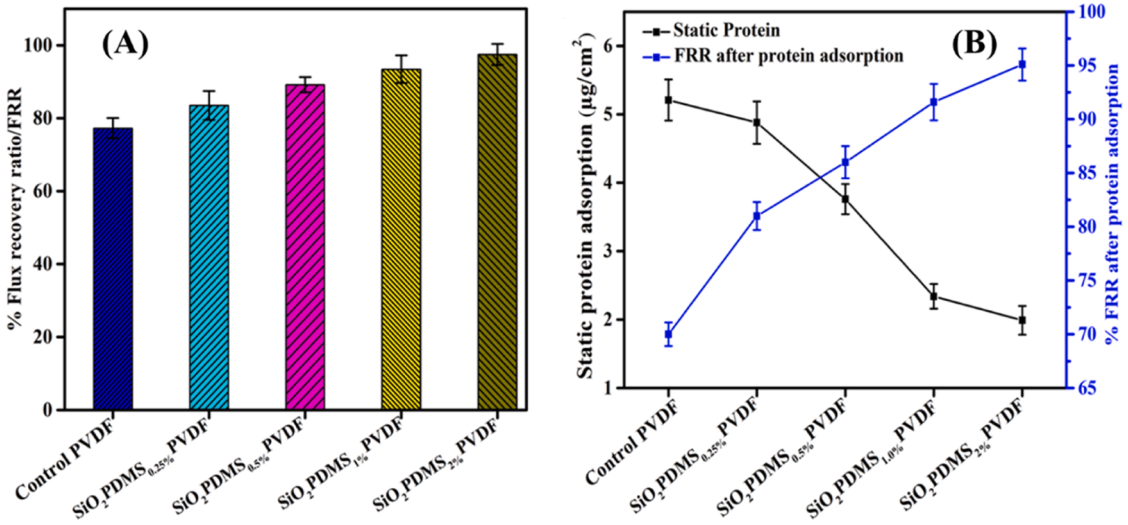

Fig. 7. (A) %FRR of control and mixed matrix PVDF membranes, (B) Static protein adsorption and %FRR of the hybrid PVDF membranes.

3.4. Anti-fouling performance of hybrid membranes

The antifouling performance of the control and PDMS-g-SiO_2-modified PVDF membranes is illustrated in Fig. 7A and B. These figures evaluate two key indicators of antifouling properties: FRR and static protein adsorption, using BSA as a model foulant.

In Fig. 7A, the FRR (%) increases consistently with the addition of PDMS-g-SiO_2 nanoparticles. Such increase surpassed that of PVDF membranes with unmodified SiO_2 (Table S1). The control PVDF membrane shows the lowest FRR, indicating higher irreversible fouling. As the concentration of PDMS-g-SiO_2 increases, the FRR gradually improves, reaching a maximum for the SiO_2PDMS$_2$ % PVDF membrane. This suggests that membranes become more resistant to fouling and are better able to recover their permeability after cleaning. The improvement in FRR is attributed to the low surface energy and fouling-resistant nature of PDMS, which provides an "omniphobic" surface. PDMS promotes weak interaction between the foulants and the membrane surface, allowing fouling layers to be more easily removed during cleaning [66, 67]. While the addition of PDMS-grafted SiO_2 nanoparticles slightly reduces the initial pure water flux due to increased mass transfer resistance and partial pore narrowing, it significantly enhances the membrane's resistance to protein fouling, as reflected by the improved flux recovery ratio (FRR). The decrease in water flux arises from a combination of higher viscosity in the casting solution and a delayed phase inversion process, which produces a denser skin layer with smaller pores (Fig. 5) (as shown in Fig. 5). At the same time, the integration of PDMS chains and hydrophilic SiO_2 domains modifies the membrane surface, forming a lubricating, low-surface-energy interface that minimizes protein adsorption and enhances interfacial compatibility. This surface modification also ensures a more uniform selective layer, contributing to higher BSA rejection. Taken together, these results highlight the inherent trade-off between permeability and antifouling performance in mixed-matrix and surface-functionalized PVDF membranes, which is consistent with previous findings reported by Zhang et al., who demonstrated that tailoring PVDF ultrafiltration membranes with oxidized low-dimensional carbon nanomaterials can simultaneously affect permeability and antifouling properties [68]. While the initial water flux is moderately reduced, the substantial gains in fouling resistance and solute selectivity justify this compromise, demonstrating that careful nanoparticle incorporation can optimize the balance between flux and antifouling performance, which is crucial for practical industrial applications.

To further corroborate the FRR trend, static protein adsorption tests were conducted to quantify the extent of BSA attachment on the membrane surface. As shown in Fig. 7B, a consistent reverse correlation is observed between PDMS-g-SiO_2 concentration and BSA adsorption. Specifically, static protein adsorption drops from 5.21 μg/cm^2 for the control PVDF to 1.99 μg/cm^2 for the SiO_2PDMS$_2$ $_{\%}$PVDF membrane. The enrichment of PDMS-g-SiO_2 chains at the membrane surface forms an omniphobic, low-fouling interface that minimizes protein adhesion and enhances desorption. Consequently, the FRR after static adsorption (Fig. 7B) values increase because foulants are more easily removed under shear forces during the washing process, confirming the fouling-release capability of PDMS-modified membranes.

Overall, the strong agreement between reduced protein adsorption and improved FRR confirms that PDMS-g-SiO_2 addition enhances the membrane's resistance to fouling and enables better recovery after exposure to protein contaminants. These outcomes align well with the previously observed reversible fouling behavior and highlight the practical benefits of incorporating PDMS-functionalized nanoparticles into ultrafiltration membranes [37].

Time-dependent flux profiles of pristine, control, and PDMS-g-SiO_2-modified PVDF membranes during the fouling cleaning cycle using 1 g/L of BSA and HA as model foulants are presented in Figure S1 (Supporting Information). At the beginning of the first filtration cycle, all membranes exhibit relatively high PWF values. The pristine PVDF membrane begins with a flux of approximately 140 LMH, whereas the control PVDF and SiO_2-modified membranes show significantly higher initial flux values. This improvement is attributed to the enhanced hydrophilicity and porosity imparted by LiCl and silica additives, which facilitate better water permeability.

As filtration progresses, flux declines sharply for all membranes due to BSA fouling (Figure S1 A), which blocks pores or forms a cake layer on the surface. The unmodified PVDF membrane shows the steepest flux decline, stabilizing at a lower value (~10 LMH), indicative of a higher degree of fouling. In contrast, the modified membranes, particularly those containing SiO_2, maintain slightly higher flux during fouling, suggesting reduced fouling affinity. After 90 min, the membranes underwent a cleaning step, followed by a second filtration cycle. The flux recovery after cleaning serves as a measure of antifouling performance. The pristine PVDF membrane exhibits limited flux recovery (~50 LMH), while PVDF+ LiCl demonstrates moderate recovery (~100 LMH). Notably, both the 0.5 % and 2.0 % SiO_2-modified membranes show superior flux recovery, regaining ~130–150 LMH, reflecting excellent antifouling and self-cleaning characteristics.Similar results were also observed for HA fouling as shown in Figure S1 B.

The superior antifouling behavior of the SiO_2PDMS-modified membranes can be attributed to a synergistic effect between the hydrophilic

SiO_2 domains and the low-surface-energy PDMS segments. The SiO_2 component enhances hydration layer formation on the membrane surface, effectively reducing hydrophobic and electrostatic interactions between HA molecules and the membrane. Meanwhile, the PDMS chains impart a lubricating, fouling-release surface that minimizes the adhesion strength of organic foulants. As a result, the fouling layer formed on these hybrid membranes is more loosely bound and can be more easily removed during hydraulic cleaning. After each fouling stage, the water-cleaning step partially restored the flux to the same level for four consecutive cycles. The SiO_2PDMS-modified membranes exhibited the highest flux recovery ratios (FRR and FRR-W), confirming that a significant portion of the foulants was reversible. This behavior demonstrates that the inclusion of SiO_2PDMS nanoparticles not only suppresses the initial adsorption of foulants but also weakens the attachment of residual foulants, facilitating their removal under mild shear during the cleaning process.

Critically, the HA fouling tests highlight the broad-spectrum antifouling capability of the SiO_2PDMS-modified PVDF membranes. While BSA primarily represents proteinaceous (hydrophilic) fouling, HA is a more complex and heterogeneous organic pollutant that includes aromatic, carboxylic, and phenolic groups. The improved performance against both foulant types confirms that the PDMS–SiO_2 modification effectively mitigates both hydrophilic and hydrophobic fouling mechanisms. This indicates that the antifouling enhancement arises not merely from increased surface hydrophilicity, but from a balanced interfacial design combining hydrophilic repulsion and hydrophobic fouling-release effects.

To further quantify the fouling mechanisms, the overall, reversible, and irreversible fouling resistances (R_t, R_r, and R_{ir}) were calculated and are summarized in Table 4. Reversible fouling R_r is due to loosely bound foulants that can be removed through physical or chemical cleaning, while irreversible fouling R_{ir} arises from strongly adhered foulants that are difficult to remove and lead to permanent performance decline. As shown in Table 5, control PVDF shows high R_r and R_{ir} values, with R_{ir} accounting for about 41 % of R_t. This implies that the membrane is more susceptible to severe, permanent fouling. However, after the inclusion of PDMS-g-SiO_2, the R_{ir} decreases significantly down to approximately 24 % for the SiO_2PDMS$_2$ % PVDF membrane while R_r increases, indicating a shift toward more manageable, reversible fouling. Similar observations were noticed with PVDF incorporated with unmodified SiO_2, but the irreversible fouling was much higher (Table S1). The R_t also declines across the modified membranes, further confirming improved resistance to foulant accumulation.

Although the reversible fouling appears higher in the hybrid membranes, this is not a drawback, it means that while some fouling still occurs, it does not compromise the long-term performance since it can be effectively removed through standard cleaning protocols. The slight increase in transmembrane pressure (TMP) required during filtration due to reduced pore size does not offset the significant gains in antifouling behavior.

In order to study the long-term antifouling stability, the long-term performance of PVDF membranes and SiO_2-PDMS modified membranes (0.5 %, 1 %, and 2 %) was evaluated over 15 days using BSA the results are presented in Figure S2. The pure PVDF membrane exhibited the highest flux decline, decreasing from 10.68 L/m^2·h on the first day to 8.98 L/m^2·h on day 15, corresponding to an approximate 16 % reduction in water flux. This steep decline indicates significant fouling due to BSA adsorption on the membrane surface and partial pore blockage. The 0.5 % SiO_2-g-PDMS membrane showed moderate antifouling behaviour, with flux decreasing gradually from 14.50 L/m^2·h to 13.28 L/m^2·h over the 15-day period, representing an approximate 8.4 % flux loss. This drop was even lower for 1 % and 2 % PDMS-g-SiO_2 of 7.4 % and 5 %, respectively. This indicates that the enhanced antifouling performance of the composite membrane is durable, underscoring its potential for real-world water treatment applications.

Table 5
Fouling resistance for control and hybrid PVDF membranes.

Membrane label	%R_t	%R_r	%R_{ir}	(R_r/R_t)	(R_{ir}/R_t)
Control PVDF	84.38	43.30	41.08	0.51	0.48
SiO_2PDMS$_{0.25\ \%}$PVDF	56.01	28.75	27.26	0.51	0.48
SiO_2PDMS$_{0.5\ \%}$PVDF	75.16	50.34	24.82	0.66	0.33
SiO_2PDMS$_{1.0\ \%}$PVDF	84.57	61.62	22.95	0.72	0.27
SiO_2PDMS$_{2.0\ \%}$PVDF	60.36	35.95	24.42	0.57	0.40

4. Comparison with previous studies

The incorporation of PDMS-g-SiO_2 into PVDF reserved the backbone structure of the latter as it was shown in the FTIR and XRD analysis suggesting that the interaction between the additives and the host polymer was likely to by a physical entanglement in the polymer chain enhanced by the hydrophobic-hydrophobic interactions between methyl groups presented in the two constituents. This is supported by the drop in the porosity and pore size upon the addition of PDMS-g-SiO_2. It is important to note that the influence of NPs on solvent and nonsolvent dynamics also contributed to the altered pore structure of the composite membrane. The partial coating of SiO_2 with PDMS endowed the nanoparticles with both hydrophobic and hydrophilic functional groups, as shown in Fig. 2A. This dual functionality enhanced foulant repulsion and promoted the formation of a hydration layer, ultimately improving water flux.

The antifouling performance of the PDMS-g-SiO_2-modified PVDF membranes developed in this study compares favourably with previously reported antifouling PVDF systems (Table 6). For instance, dip-coated PVDF/PDMS-g-PEG membranes exhibited FRR values around 95 % due to the combined effects of hydrophilic PEG and low-surface-energy PDMS chains [62], while PEG-modified PVDF membranes also showed high flux recovery and reduced protein adhesion through enhanced hydrophilicity [63]. Similarly, nanohybrid incorporation of SiO_2@GO into PVDF achieved an FRR of 96 % and lowered protein adsorption from 138.7 to 62.4 μg cm^{-2}, attributed to the improved surface energy and interfacial hydration [64].

Zwitterionic surface modifications such as poly(sulfobetaine methacrylate) (PSBMA) and carboxybetaine (CBMA) grafting have also been reported to impart excellent antifouling behaviour by forming strong hydration layers on the surface of membranes and achieving high FRR values (93–96 %). However, both approaches typically involve complex synthetic steps and may suffer from limited chemical durability under long-term operation.

In comparison, the present PDMS-g-SiO_2 modified PVDF membranes achieved an FRR of 97.5 % and reduced BSA adsorption dramatically from 5.1 to 1.99 μg cm^{-2}, outperforming most of the reported systems. This superior performance arises from the synergistic contribution of the hydrophilic SiO_2 core and omniphobic PDMS shell, which together form a lubricating, low-surface-energy interface that reduces foulant adhesion while facilitating easy cleaning. The results confirm the successful integration of antifouling and fouling-release mechanisms and demonstrate that this simple nanoparticle blending strategy achieves comparable or higher flux recovery with significantly lower protein adsorption than PEG-based, zwitterionic, or other nanohybrid PVDF membranes, offering a scalable and durable solution for practical ultrafiltration applications.

5. Conclusion

Mixed matrix PVDF membranes were fabricated via traditional NIPS using PDMS-g-SiO_2 as nano additives. PDMS-g-SiO_2 NPs were successfully synthesized using PDMS with single terminal hydroxyl via steglich esterification which reported for the first time in this study. The nanoparticles were able to enhance the anti-fouling properties of mixed matrix PVDF membranes by improving the % FRR ratio. The hybrid

Table 6
Comparison of the antifouling performance of PDMS-g-SiO_2/PVDF in this study with previously reported PVDF-based membranes.

Membrane Type	Modification method	%FRR	Protein Adsorption (μg/cm²)	Key Notes/Observation	References
PVDF/PDMS-g-PEG	Dip-coating with amphiphilic polymer	~95 %	Low BSA adsorption from 52 to 18, improved by 65 %	Dual-mode antifouling via PEG and PDMS	[69]
PVDF/PEG	Surface anchoring	High FRR (90 % compared to pristine 50 %)	Significantly reduced BSA adsorption	Improved antifouling performance by 80 %	[70]
PVDF/SiO_2@GO	Nanohybrid incorporation	96 %	138.7 to 62.4 **(μg/cm²), improved by 55 %**	Enhanced surface hydrophilicity	[71]
PVDF/SiO_2-g-PDMS	Nanoparticle embedding	~94 %	Reduced BSA and HA adsorption from 45 to 19 **(μg/cm²), improved by 58 %**	Enhanced fouling resistance	[37]
PVDF/SBMA	Sonication followed by an ozone method	**88.9 %/100 %**	Reduced BSA from 25 μg/cm² to 1 μg/cm², improved by 96 %	Excellent antifouling performance	Chiang et al.,2009 [72]
Zwitterionic SiO_2 nanoparticles blended into PVDF UF membranes	Blend of amino-acid-based zwitterionic SiO_2 into PVDF via NIPS	(FRR) > 95 % for BSA/HA fouling tests	Static BSA adsorption decreased to ~10 μg/cm²	Improved antifouling performance	Zhu et al.,2016 [73]
Zwitterionic polymer brush (poly-(lysine methacrylamide)) grafted onto PVDF membranes	Surface-initiated ATRP to graft zwitterionic brush on PVDF	~95 %	BSA adsorption decreased from 52 to ~10 μg/cm², improved by 81 %	Improved antifouling performance	Liu et al.,2016 [74]
Zwitterionic organosilica coating on PVDF microfiltration membrane	Sol-gel coating of novel zwitterionic organosilica monomer on PVDF	After three fouling cycles: flux recovery for protein ~67.8 %, for polysaccharide ~90.7 %; excellent anti-biofouling	BSA adsorption reduced from 52 to 8, improved by 84.6 %	exhibited excellent and long-term antifouling ability. outstanding anti-bioadhesion ability	Song et al., 2018[75]
SiO_2PDMSPVDF	**Nanoparticle blending**	**97.5 %**	**From 5.1 to 1.99 (μg/cm²), improved by 61.8 %**	**Superior antifouling performance via synergistic PDMS–SiO_2 interface**	**This study**

membranes exhibited lower BSA protein adsorption on their surface during static protein adsorption test. Due to the added PDMS-g-SiO_2, the ratio of R_r/R_t increased. This indicates that the BSA molecules adsorbed on the top surface of hybrid PVDF membranes was more easily washed off during cleaning. These improvements were achieved at the expense of slight loss in pure water flux. These results are of particular importance to the ultrafiltration applications in water and wastewater treatment industry. The positive antifouling properties bestowed by PDMS-g-SiO_2 warrant further investigation for their tolerance against other types of fouling such as organic and biological which would be an important future work goal.

Funding

This research did not receive any specific grant from funding agencies in the public, commercial, or not-for-profit sectors.

CRediT authorship contribution statement

Muayad Al-Shaeli: Writing – review & editing, Writing – original draft, Visualization, Validation, Methodology, Formal analysis, Data curation, Conceptualization. **Raed A. Al-Juboori:** Writing – review & editing, Formal analysis. **Huanting Wang:** Supervision. **Bradley Ladewig:** Writing – review & editing, Visualization, Supervision, Project administration, Methodology, Conceptualization. **Qusay F. Alsalhy:** Visualization, Conceptualization. **Jianhua Zhang:** Visualization, Conceptualization.

Declaration of competing interest

The authors declare that they have no known competing financial interests or personal relationships that could have appeared to influence the work reported in this paper.

Supplementary materials

Supplementary material associated with this article can be found, in the online version, at doi:10.1016/j.ceja.2025.100991.

Data availability

Data will be made available on request.

References

[1] X. Yin, et al., Ultra-fine electrospun nanofibrous membranes for multicomponent wastewater treatment: filtration and adsorption, Sep. Purif. Technol. 242 (2020) 116794.
[2] S. Hube, et al., Direct membrane filtration for wastewater treatment and resource recovery: a review, Sci. Total Environ. 710 (2020) 136375.
[3] J. Hong, Y. He, Polyvinylidene fluoride ultrafiltration membrane blended with nano-ZnO particle for photo-catalysis self-cleaning, Desalination 332 (1) (2014) 67–75.
[4] R. Mishra, et al., Chapter 12 - current status of available techniques for removal of heavy metal contamination in the river ecosystem, in: S. Madhav, et al. (Eds.), Ecological Significance of River Ecosystems, Elsevier, 2022, pp. 217–234.
[5] V. Potapov, R. Fediuk, D. Gorev, Membrane concentration of hydrothermal SiO_2 nanoparticles, Sep. Purif. Technol. 251 (2020) 117290.
[6] Y. Huang, X. Feng, Polymer-enhanced ultrafiltration: fundamentals, applications and recent developments, J. Memb. Sci. 586 (2019) 53–83.
[7] T. Ahmad, C. Guria, A. Mandal, A review of oily wastewater treatment using ultrafiltration membrane: a parametric study to enhance the membrane performance, J. Water Process Eng. 36 (2020) 101289.
[8] P.D. Peeva, et al., Cross-flow ultrafiltration of protein solutions through unmodified and surface functionalized polyethersulfone membranes – Effect of process conditions on separation performance, Sep. Purif. Technol. 92 (2012) 83–92.
[9] H. Susanto, et al., Preparation of low-fouling polyethersulfone ultrafiltration membranes by incorporating high-molecular-weight chitosan with the help of a surfactant, S. Afr. J. Chem. Eng. 33 (2020) 133–140.
[10] B. Liu, et al., Ultrafiltration pre-oxidation by boron-doped diamond anode for algae-laden water treatment: membrane fouling mitigation, interface characteristics and cake layer organic release, Water Res. 187 (2020) 116435.
[11] F. Qu, et al., Membrane fouling control by UV/persulfate in tertiary wastewater treatment with ultrafiltration: a comparison with UV/hydroperoxide and role of free radicals, Sep. Purif. Technol. 257 (2021) 117877.

[12] Y. Su, et al., Modification of polyethersulfone ultrafiltration membranes with phosphorylcholine copolymer can remarkably improve the antifouling and permeation properties, J. Memb. Sci. 322 (1) (2008) 171–177.
[13] S. Jiang, Y. Li, B.P. Ladewig, A review of reverse osmosis membrane fouling and control strategies, Sci. Total Environ. 595 (2017) 567–583.
[14] Z. Ren, et al., Ferrous-activated sodium percarbonate pre-oxidation for membrane fouling control during ultrafiltration of algae-laden water, Sci. Total Environ. 739 (2020) 140030.
[15] H. Yu, et al., Hydrothermal carbon nanospheres assisted-fabrication of PVDF ultrafiltration membranes with improved hydrophilicity and antifouling performance, Sep. Purif. Technol. 247 (2020) 116889.
[16] J. Zhu, et al., PVDF mixed matrix ultrafiltration membrane incorporated with deformed rebar-like Fe3O4–palygorskite nanocomposites to enhance strength and antifouling properties, J. Memb. Sci. 612 (2020) 118467.
[17] X. Chen, et al., Functional PVDF ultrafiltration membrane for tetrabromobisphenol-A (TBBPA) removal with high water recovery, Water Res. 181 (2020) 115952.
[18] Z. Wang, et al., Hot-pressed PAN/PVDF hybrid electrospun nanofiber membranes for ultrafiltration, J. Memb. Sci. 611 (2020) 118327.
[19] S. Jiang, B.P. Ladewig, Green synthesis of polymeric membranes: recent advances and future prospects, Curr. Opin. Green Sustain. Chem. 21 (2020) 1–8.
[20] J.F. Hester, P. Banerjee, A.M. Mayes, preparation of protein-pesistant purfaces on poly(vinylidene fluoride) pembranes via purface pegregation, Macromolecules 32 (5) (1999) 1643–1650.
[21] J.F. Hester, A.M. Mayes, Design and performance of foul-resistant poly(vinylidene fluoride) membranes prepared in a single-step by surface segregation, J. Memb. Sci. 202 (1–2) (2002) 119–135.
[22] S. Roy, D.V. Bhalani, S.K. Jewrajka, Surface segregation of segmented amphiphilic copolymer of poly(dimethylsiloxane) and poly(ethylene glycol) on poly(vinylidene fluoride) blend membrane for oil–water emulsion separation, Sep. Purif. Technol. 232 (2020) 115940.
[23] Y. Chang, et al., Surface grafting control of PEGylated poly(vinylidene fluoride) antifouling membrane via surface-initiated radical graft copolymerization, J. Memb. Sci. 345 (1) (2009) 160–169.
[24] S. Chen, et al., Strong resistance of phosphorylcholine self-assembled monolayers to protein adsorption: insights into nonfouling properties of zwitterionic materials, J. Am. Chem. Soc 127 (41) (2005) 14473–14478.
[25] L. Zhou, et al., Preparation of double-responsive SiO_2-g-PDMAEMA nanoparticles via ATRP, Mater. Lett. 62 (8) (2008) 1372–1375.
[26] X. Zhao, et al., Engineering amphiphilic membrane surfaces based on PEO and PDMS segments for improved antifouling performances, J. Memb. Sci. 450 (2014) 111–123.
[27] M. Lejars, A. Margaillan, C. Bressy, Fouling release coatings: a nontoxic alternative to biocidal antifouling coatings, Chem. Rev. 112 (8) (2012) 4347–4390.
[28] J. Zhao, et al., Biomimetic and bioinspired membranes: preparation and application, Prog. Polym. Sci. 39 (9) (2014) 1668–1720.
[29] J.E. Mark, Some interesting things about polysiloxanes, Acc. Chem. Res 37 (12) (2004) 946–953.
[30] M.J. Owen, Low surface energy inorganic polymers, Comments Inorg. Chem. 7 (4) (1988) 195–213.
[31] H.S. Sundaram, et al., Fluorinated amphiphilic polymers and pheir plends for pouling-pelease ppplications: the penefits of a triblock copolymer surface, ACS. Appl. Mater. Interfaces 3 (9) (2011) 3366–3374.
[32] H.S. Sundaram, et al., Fluorine-free mixed amphiphilic polymers based on PDMS and PEG side chains for fouling release applications, Biofouling 27 (6) (2011) 589–602, https://doi.org/10.1080/08927014.2011.587662.
[33] S.S. Madaeni, S. Zinadini, V. Vatanpour, Preparation of superhydrophobic nanofiltration membrane by embedding multiwalled carbon nanotube and polydimethylsiloxane in pores of microfiltration membrane, Sep. Purif. Technol. 111 (2013) 98–107.
[34] M.S. Rahaman, et al., Control of biofouling on reverse osmosis polyamide membranes modified with biocidal nanoparticles and antifouling polymer brushes, J. Mater. Chem. B 2 (12) (2014) 1724–1732.
[35] K. Kannan, et al., Accumulation of perfluorooctane sulfonate in marine mammals, Env. Sci. Technol 35 (8) (2001) 1593–1598.
[36] W. D'Hollander, et al., Characterisation of perfluorooctane sulfonate (PFOS) in a terrestrial ecosystem near a fluorochemical plant in Flanders, Belgium, Environ. Sci. Pollut. Res. 21 (20) (2014) 11856–11866.
[37] H. Wang, X. Zhao, C. He, Enhanced antifouling performance of hybrid PVDF ultrafiltration membrane with the dual-mode SiO2-g-PDMS nanoparticles, Sep. Purif. Technol. 166 (2016) 1–8.
[38] H. Wu, J. Mansouri, V. Chen, Silica nanoparticles as carriers of antifouling ligands for PVDF ultrafiltration membranes, J. Memb. Sci. 433 (2013) 135–151.
[39] C.A. Smolders, et al., Microstructures in phase-inversion membranes. Part 1. Formation of macrovoids, J. Memb. Sci. 73 (2–3) (1992) 259–275.
[40] F. Pardal, V. Lapinte, J.-J. Robin, Modification of silica nanoparticles by grafting of copolymers containing organosilane and fluorine moities, J. Polym. Sci. A: Polym. Chem. 47 (18) (2009) 4617–4628.
[41] C. Bartholome, et al., Nitroxide-mediated polymerizations from silica nanoparticle surfaces: "graft from" polymerization of styrene using a triethoxysilyl-terminated alkoxyamine initiator, Macromolecules 36 (21) (2003) 7946–7952.
[42] C. Feng, et al., Factors affecting pore structure and performance of poly(vinylidene fluoride-co-hexafluoro propylene) asymmetric porous membrane, J. Memb. Sci. 277 (1) (2006) 55–64.
[43] N. Li, et al., Preparation and properties of PVDF/PVA hollow fiber membranes, Desalination 250 (2) (2010) 530–537.
[44] C.M. Tam, A.Y. Tremblay, Membrane pore characterization—comparison between single and multicomponent solute probe techniques, J. Memb. Sci. 57 (2) (1991) 271–287.
[45] E. Yuliwati, et al., Effect of modified PVDF hollow fiber submerged ultrafiltration membrane for refinery wastewater treatment, Desalination 283 (2011) 214–220.
[46] Q. Shi, et al., Zwitterionic polyethersulfone ultrafiltration membrane with superior antifouling property, J. Memb. Sci. 319 (1) (2008) 271–278.
[47] S.P. Nunes, M.L. Sforça, K.-V. Peinemann, Dense hydrophilic composite membranes for ultrafiltration, J. Memb. Sci. 106 (1) (1995) 49–56.
[48] J.T. Park, et al., Surface modification of silica nanoparticles with hydrophilic polymers, J. Ind. Eng. Chem. 16 (4) (2010) 517–522.
[49] B. Jung, Preparation of hydrophilic polyacrylonitrile blend membranes for ultrafiltration, J. Memb. Sci. 229 (1) (2004) 129–136.
[50] A. Isakova, et al., Diels–Alder cycloaddition and RAFT chain end functionality: an elegant route to fullerene end-capped polymers with control over molecular mass and architecture, Polym. Chem. 8 (18) (2017) 2796–2805.
[51] M. Yu, et al., Effect of particle modification on the shear thickening behaviors of the suspensions of silica nanoparticles in PEG, Colloid. Polym. Sci. 296 (11) (2018) 1767–1776.
[52] B. Cho, D. Kim, T. Kim, Exceptional properties of hyper-resistant armor of a hydrothermal vent crab, Sci. Rep. 12 (1) (2022) 11816.
[53] M.A. Wahab, I.I. Kim, C.-S. Ha, Hybrid periodic mesoporous organosilica materials prepared from 1,2-bis(triethoxysilyl)ethane and (3-cyanopropyl)triethoxysilane, Microporous Mesoporous Mater. 69 (1) (2004) 19–27.
[54] A. Cassano, M. Marchio, E. Drioli, Clarification of blood orange juice by ultrafiltration: analyses of operating parameters, membrane fouling and juice quality, Desalination 212 (1–3) (2007) 15–27.
[55] R. Ellerbrock, M. Stein, J. Schaller, Comparing amorphous silica, short-range-ordered silicates and silicic acid species by FTIR, Sci. Rep. 12 (1) (2022) 11708.
[56] L.M. Johnson, et al., Elastomeric microparticles for acoustic mediated bioseparations, J. Nanobiotechnology. 11 (1) (2013) 22.
[57] M.A. Hari, et al., Flexible and self-powered PVDF-nanosilica based piezoelectric touch sensor, SN Comput. Sci. 4 (1) (2022) 64.
[58] H. Mahdavi, et al., Preparation of high-performance PVDF mixed matrix membranes incorporated with PVDF-g-PMMA copolymer and GO@SiO_2 nanoparticles for dye rejection applications, J. Water Process Eng. 46 (2022) 102560.
[59] C. Liao, et al., Synthesis and characterization of low content of different SiO_2 materials composite poly (vinylidene fluoride) ultrafiltration membranes, Desalination 285 (2012) 117–122.
[60] S. Gupta, P.C. Ramamurthy, G. Madras, Synthesis and characterization of silicone polymer/functionalized mesostructured silica composites, Polym. Chem. 2 (11) (2011) 2643–2650.
[61] C.R. Tanardi, et al., PDMS grafting of mesoporous γ-alumina membranes for nanofiltration of organic solvents, J. Memb. Sci. 469 (2014) 471–477.
[62] X. Wang, et al., Adsorption of bovine serum albumin on silver surfaces enhances the release of silver at pH neutral conditions, Phys. Chem. Chem. Phys. 17 (28) (2015) 18524–18534.
[63] L. Dalstein, E. Potapova, E. Tyrode, The elusive silica/water interface: isolated silanols under water as revealed by vibrational sum frequency spectroscopy, Phys. Chem. Chem. Phys. 19 (16) (2017) 10343–10349.
[64] E. Suryawirawan, et al., Bovine serum albumin rejection by an open ultrafiltration membrane: characterization and modeling, Membr. (Basel) 14 (1) (2024) 26.
[65] M. Jafari, A. Vatani, T. Mohammadi, CFD modeling of braid-reinforced hollow fiber membranes for efficient water and bovine serum albumin (BSA) separation, J. Water Process Eng. 65 (2024) 105746.
[66] Z. Li, et al., Fabrication of photocurable liquid-like easy-cleaning coatings based on a polydimethylsiloxane-modified silicone resin, Prog. Org. Coat. 187 (2024) 108169.
[67] Y. Yue, Design of Porous Polydimethylsiloxane For Non-Fouling Filtration, University of Toronto (Canada), Canada Ontario, CA, 2023, p. 132.
[68] J. Zhang, et al., Improved hydrophilicity, permeability, antifouling and mechanical performance of PVDF composite ultrafiltration membranes tailored by oxidized low-dimensional carbon nanomaterials, J. Mater. Chem. A 1 (9) (2013) 3101–3111.
[69] Y. Chen, X. Zhao, C. He, Dual-mode antifouling ability of PVDF membrane with a surface-anchored amphiphilic polymer, RSC Adv. 5 (84) (2015) 68998–69005.
[70] X. Zhao, H. Xuan, C. He, Enhanced separation and antifouling properties of PVDF ultrafiltration membranes with surface covalent self-assembly of polyethylene glycol, RSC Adv. 5 (99) (2015) 81115–81122.
[71] Z.-K. Li, et al., Preparation and properties of PVDF/SiO_2@GO nanohybrid membranes via thermally induced phase separation method, J. Memb. Sci. 511 (2016) 151–161.
[72] Y.-C. Chiang, et al., Sulfobetaine-grafted poly(vinylidene fluoride) ultrafiltration membranes exhibit excellent antifouling property, J. Memb. Sci. 339 (1) (2009) 151–159.
[73] J. Zhu, X. Zhao, C. He, Zwitterionic SiO_2 nanoparticles as novel additives to improve the antifouling properties of PVDF membranes, RSC Adv. 5 (66) (2015) 53653–53659.
[74] D. Liu, et al., Antifouling PVDF membrane grafted with zwitterionic poly(lysine methacrylamide) brushes, RSC Adv. 6 (66) (2016) 61434–61442.
[75] W. Song, et al., Facile sol-gel coating process for anti-biofouling modification of poly (vinylidene fluoride) microfiltration membrane based on novel zwitterionic organosilica, J. Memb. Sci. 550 (2018) 266–277.